# High resolution metrology of autoionizing states through Raman interferences

A. Plunkett $^1$ , J. K. Wood $^3$ , M. A. Alarcón $^2$ , D. Biswas $^1$ , C. H. Greene $^2$ , A. Sandhu $^{1,3}$ 

E-mail: asandhu@arizona.edu

Abstract. Metrology of electron wavepackets is often conducted with the technique of photoelectron interferometry. However, the ultrashort light pulses employed in this method place a limit on the energy resolution. Here, weadvance ultrafast photoelectron interferometry access both high temporal and spectral resolution. The key to our approach lies in stimulating Raman interferences with a probe pulse and while monitoring the modification of the autoionizing electron yield in a separate delayed detection step. As a proof of the principle, we demonstrated this technique to obtain the components of an autoionizing nf' wavepacket between the spin-orbit split ionization thresholds in argon. We extracted the amplitudes and phases from the interferogram and compared the experimental results with second-order perturbation theory calculations. This high resolution probing and metrology of electron dynamics opens the path for study of molecular wavepackets.

### 1. Introduction

In the fields of femtosecond and attosecond science [1, 2] photoelectron wavepacket interferometry is a well established technique for wavepacket metrology [3, 4, 5]. A complete characterization of an excited wave packet can be used to probe strong field effects [6, 7], autoionization dynamics [8, 9, 10], and molecular processes [11]. In these pump-probe experiments, one first prepares the excited state wavepacket using a broadband, femtosecond or attosecond pump pulse, followed by a sufficiently broad band ionizing probe pulse. Due to interference between pathways to the same final continuum state, quantum beats in the kinetic energy spectrum of ionized electrons are seen. From this interference pattern, when sampled over many probe delays, one can extract amplitude and phases of constituent wavepacket components using Fourier methods. In order to probe temporal dynamics on increasingly short timescales, one needs increasingly short laser pulses. However, this typically comes at a cost, for the increase in the time resolution leads to a corresponding decrease in the energy resolution, as indicated by the well-known uncertainty relation  $\delta t \, \delta E \geq \hbar/2$ . When the wavepacket is a superposition of large set of states, reconstructing the wavepacket from a complex spectrogram can be challenging, as muliple states can beat with very similar frequencies. Increasing the range of scans to obtain higher Fourier frequency resolution to distinguish nearby beats becomes prohibitive at some point. We previously presented [12] a method which bypasses this limitation by using a probing pulse

<sup>&</sup>lt;sup>1</sup>Department of Physics, University of Arizona, Tucson, Arizona 85721, USA

<sup>&</sup>lt;sup>2</sup>Department of Physics and Astronomy, Purdue University, West Lafayette, Indiana 47907, USA

<sup>&</sup>lt;sup>3</sup>College of Optical Sciences, University of Arizona, Tucson, Arizona 85721, USA

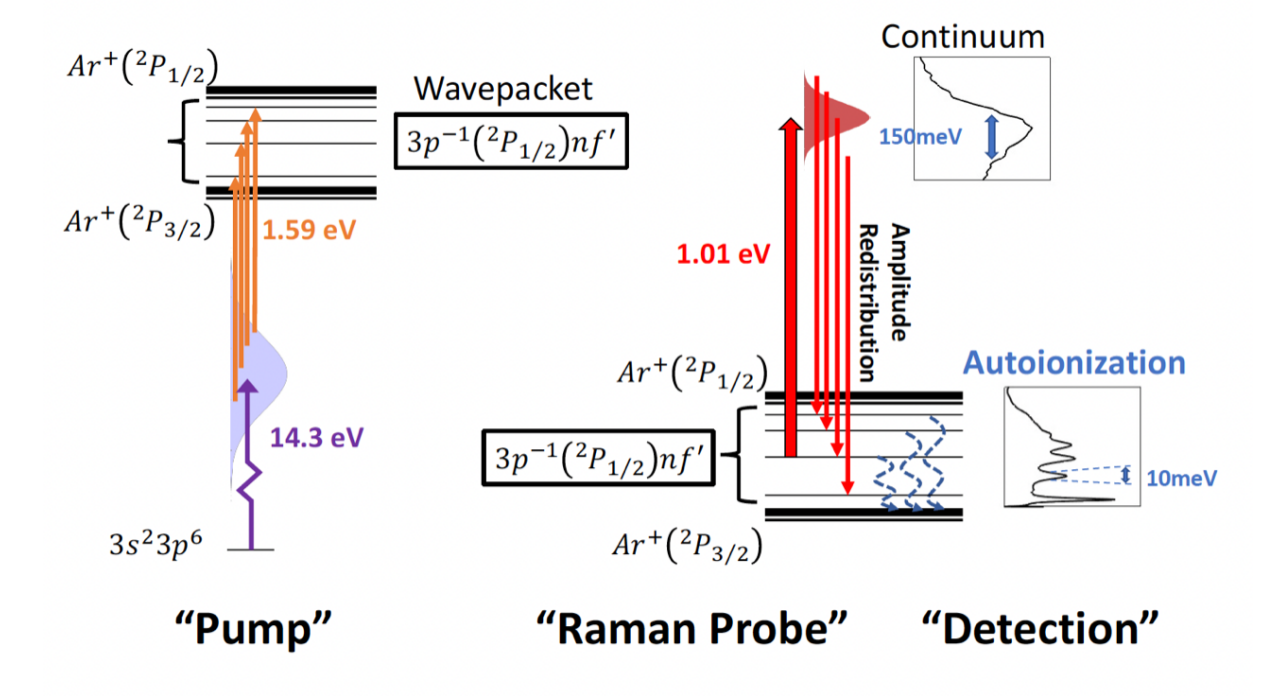


Figure 1. Energy level diagram depicting the "pump" and "probe" steps of this femtosecond spectroscopy method. The "probe" consists of a two-color excitation of autoionizing nf' states. The "probe" step is a two photon coherent amplitude redistribution between nf' states. Only one amplitude redistribution step is depicted for clarity, but this redistribution will in general occur at every constituent of the wavepacket. In contrast to the direct photoionization, the delayed detection of autoionization signal yield high energy resolution.

that stimulates Raman interferences between the constituent components of the wavepacket, followed by a delayed detection through autoionization. Here, we extend our previous work by conducting additional analysis, namely the extraction of experimental amplitudes and phases of the quantum beat signals from the difference spectrogram, followed by comparison with the theoretical calculations. We observe that the amplitudes agree between theory and experiment, while the phases of quantum beats show a phase offset.

#### 2. Method

The three color experiment begins with an approximately 2mJ, 40fs, 1KHz, linearly polarized, 780nm beam which is split on a 50/50 beamsplitter into two arms. One arm proceeds to an optical parametric amplifier (OPA), tuned to produce a 1200nm linearly polarized pulse with comparable pulse width, which henceforth is referred to as probe. The second arm that is focused into Xe gas for HHG production of odd harmonics 9-19 of the fundamental 780nm (1.6eV) driving pulse. A small amount of of the 780nm beam that drives the HHG process makes through the Xe gas cell, and copropagates with the XUV attosecond pulse train, arriving coincidentally at the target. This two-color beam, henceforth referred to as pump, is focused into an effusive jet of argon gas in the Velocity Map Imaging (VMI) chamber via a grazing incidence toroidal mirror. As depicted in the pump step of figure 1, the 9th harmonic (14.3eV) and coincident fundamental (1.6eV) photons coherently excite an optically dark wavepacket composed of nf'

 $(n \geq 9)$  states which are situated in the continuum of  $[^2P_{3/2}]$  ion core but energetically bound to the  $[^2P_{1/2}]$  core. Due to configuration interaction, these states relax via autoionization, releasing the Rydberg electron to the continuum of the  $[^2P_{3/2}]$  ion core. Long lifetimes of the nf' series produce sharp energetic peaks ( $\sim 10 \text{meV}$ ) compared to broad bandwidth ( $\sim 150 \text{ meV}$ ) of direct photoelectrons ejected into the continuum.

The probe arm navigates a time delayed path and is focused with a 50cm lens ( $\sim 1 \text{ TW/cm}^2$  at target) before recombining with pump beam line on a mirror with a hole. Both pump and probe are linearly polarized in the plane perpendicular to VMI spectrometer axis. As depicted in the probe step of figure 1, the time delayed  $\sim 60 \text{fs}$  probe pulse (1 eV) stimulates Raman transitions between the constituents of the wavepacket, thus redistributing the wavepacket amplitudes.

We obtain the photoelectron and autoionizing electron spectra for a range of probe delays in steps of 2 fs. At each time delay, we plot the a differential yield signal by subtracting pump + probe spectra from pump alone spectra, as seen in figure 2 spectrogram. The beats in the signal result from the interference in the autoionization channel, due to the redistribution of the amplitudes between the nf' states by the Raman probe. The high energy resolution along the y-axis is obtained due to the long autoionization timescales in our detection step.

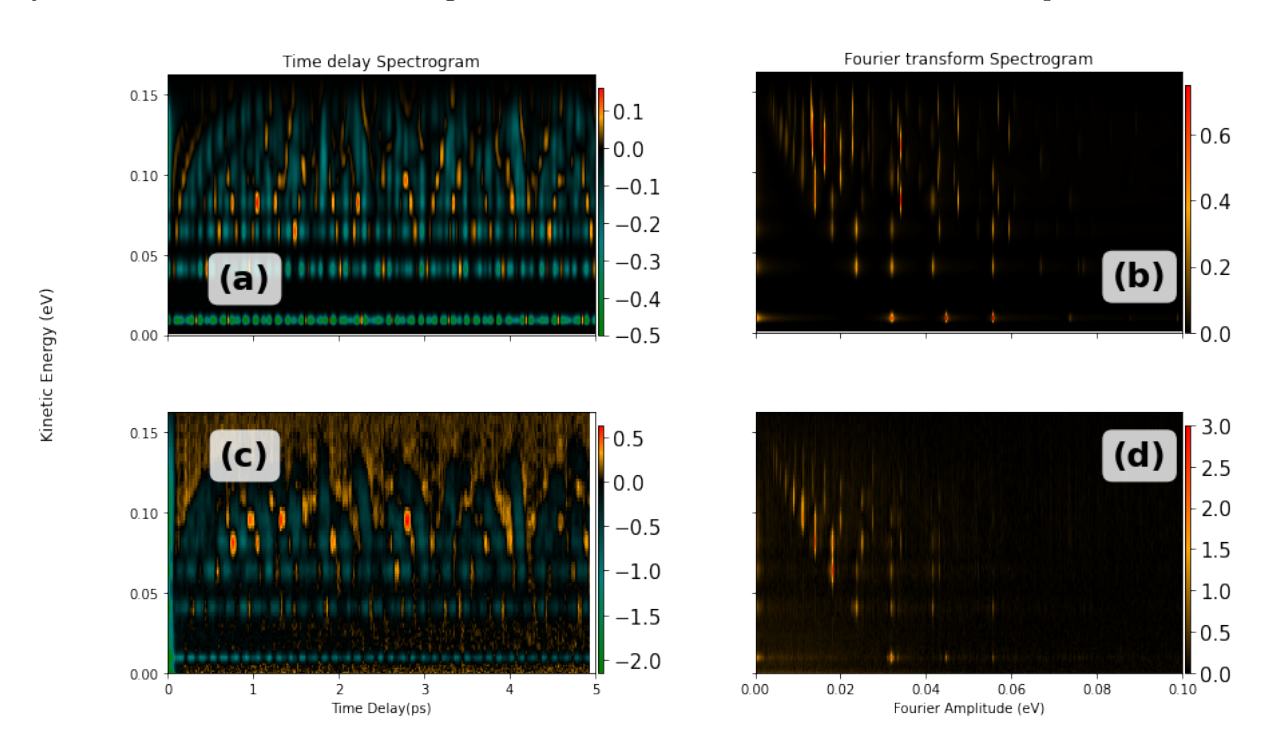


Figure 2. Differential electron spectrograms corresponding to the autoionizing nf' wavepacket. Panels a and c on the left show difference spectrogram (pump+probe - pump) as a function of time delay of probe pulse. Green indicates depletion of electron yield at that energy due to probe pulse, whereas red indicates enhancement. Panels b and d on the right show the amplitude of the Fourier transform of the signal. Panels a and b are theoretical calculation while c and d are experimental signals.

## 3. Analysis

Tools from multichannel quantum defect theory (MQDT) and second order time-dependent perturbation theory are used to model the light-matter interaction. Following the two color pump the states that are excited are autoionizing states with even symmetry and total angular momentum equal to 0 or 2. This restricts to states with an outer electron with orbital angular momentum l=1 or l=3. Using the MQDT parameters from Pellarin et al [13] we determined the width and position of autoionizing resonances with total J=2 for both p' and f' states [14, 15] and found the excitation to f' states dominated by  $\sim$ 2 orders of magnitude. Thus, neglecting the p' states is a good approximation.

Given that the f' states have a very small quantum defect and are very narrow, through their interactions with the light pulse their wave function can be approximated by the bound part only, with a hydrogenic radial wave function.

The initial wave packet is then given by

$$|\Psi_o\rangle = \mathcal{A} \sum_n A_n |\psi_n\rangle = \mathcal{A} \sum_n A_n \frac{u_{n,3}(r)}{r} \Phi_{1/2}^{J=2},$$
 (1)

where  $\Phi_{j_c}^{J=2} = \chi_{j_c} |\{[(\ell_c, s_c)j_c, s]J_cs, \ell\}J, M\rangle$  is the Jcs coupled angular momentum atomic state[16], with an ionic core of angular momentum  $j_c$ , ionic wave function  $\chi_{j_c}$ , and total angular momentum J. the operator  $\mathcal{A}$  is the antisymmetrization operator that is trivially realized since the electrons are in different regions of space. The state  $|\psi_n\rangle$  is the bound part of the autoionizing f' state with principal quantum number n.

The corresponding probability amplitude for each nf' state after interaction with SWIR pulse is based on the perturbative expansion of the transition operator as in Chapter 2 of [17] using a time-dependent peturbation of the form

$$V(t) = \mathcal{E}_o e^{-((t-t_o)/\gamma)^2} \cos(\omega t) \hat{\epsilon} \cdot \vec{r}, \tag{2}$$

where  $\mathcal{E}_o$  is SWIR field strength, central frequency  $\omega$ , polarization  $\hat{\epsilon}$ , time delay  $t_o$  and temporal intensity FWHM of  $\gamma\sqrt{2\ln 2}$ . Calculating the correction to the population of the autoionizing state  $|\psi_f\rangle$  with this perturbation gives

$$\left| \left\langle \psi_f | T | \Psi_o \right\rangle \right|^2 = \left| A_f \right|^2 + \operatorname{Re} \left\{ A_f^* \left\langle \psi_f \left| T^{(2)} \right| \psi_o \right\rangle \right\} + O\left(\mathcal{E}_o^4\right). \tag{3}$$

removing the effects of the pump is equivalent to subtracting the initial amplitude  $|A_f|^2$  from this probability, therefore the theoretical estimate for the effects of the probe is:

$$D_f(t_o) = \operatorname{Re}\left\{A_f^* \left\langle \psi_f \left| T^{(2)} \right| \psi_o \right\rangle \right\} + O\left(\mathcal{E}_o^4\right). \tag{4}$$

The matrix elements of the second order transition operator,  $T^{(2)}$ , is a sum over all the autoionizing states of the form:

$$\left\langle \psi_f \left| T^{(2)} \right| \psi_o \right\rangle = -\sum_n A_n \mathcal{E}_o^2 \exp\left\{ -\gamma^2 \frac{\left( E_f - E_n \right)^2}{8} + i \left( E_f - E_n \right) t_o \right\} \mathcal{Z}_{nf}, \tag{5}$$

where the term  $\mathcal{Z}_{nf}$  involves an integral-sum over the dipole matrix elements between the autoionizing states and the continuum of intermediate states weighted by a coefficient related to the spectral profile of the probe pulse.

After the pulse is over, it is assumed that the totality of the amplitude in the bound state will have decayed to the detector and will be observed across the predicted width of the resonance. Figure 2 is obtained by extending the expression in equation 4 with a lorentzian over the width of the resonance and then convolving over the resolution of the experimental apparatus. As previously noted, the color indicates either a positive (red) or negative (green) change in electron yield at the relevant electron energy due to probe interaction.

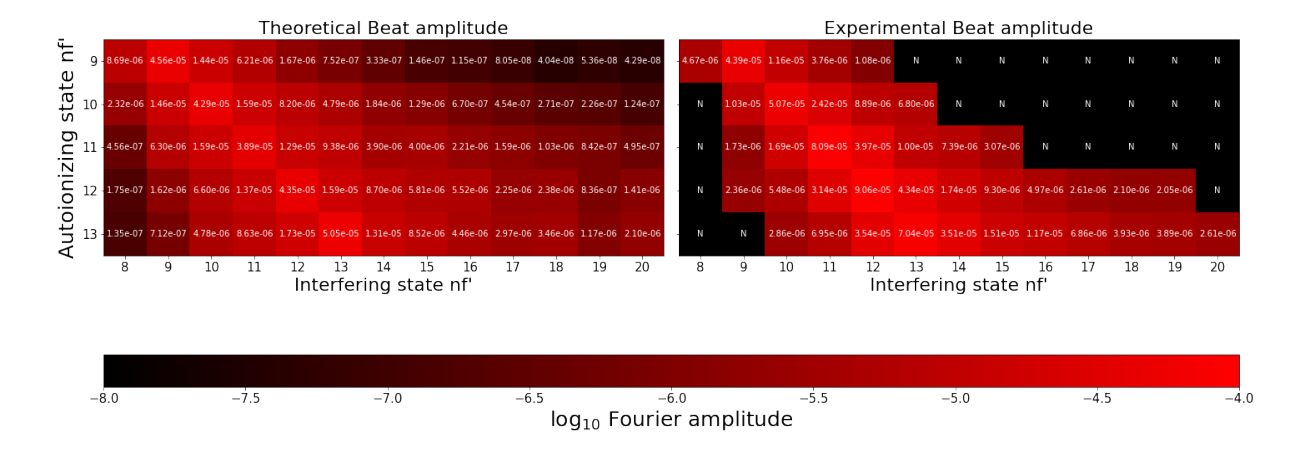


**Figure 3.** Amplitude of the quantum beats selected from FFT, in both experiment and theory. The colormap is logarithmic and each square has a label with the value, with N assigned to the beat values that are below the noise level. Experimental FFT by selecting only the values in the 70th percentile. Beat amplitudes are concentrated around the diagonal and diffuse as the separation in principal quantum number grows. Both experiment and theory show agreement.

Each nf' autoionization signal, of which n=9-13 are clearly resolved, exhibit oscillation frequencies corresponding to pairs of autoionizing states. Within the bandwidth of the interfering laser pulse, any given state can pair-up with any other state, leading to a very large number of beat frequencies even when considering relatively few participating states. This point makes it possible to propose a method to extract a the relative amplitude of the states in the wave packet and have a more quantative comparison between experiment and theory.

To see this, let us take the fourier transform of the correction in equation 4

$$\tilde{\mathcal{D}}_{f}(\omega) = -\mathcal{E}_{o}^{2} |A_{f}|^{2} \mathcal{Z}_{ff} \delta(\omega) - \frac{\mathcal{E}_{o}^{2}}{2} \sum_{n \neq f} \exp \left\{ -\gamma^{2} \frac{(E_{f} - E_{n})^{2}}{8} \right\} \qquad \left[ A_{f}^{*} A_{n} \mathcal{Z}_{nf} \delta(E_{f} - E_{n} - \omega) + A_{f} A_{n}^{*} \mathcal{Z}_{nf}^{*} \delta(E_{f} - E_{n} + \omega) \right]$$

$$(6)$$

The coefficients that accompany the delta functions have specific symmetric properties with respect to the combination of different principal quantum numbers. Choose  $\alpha > \beta$  such that the terms that correspond to the positive frequency  $\omega = E_{\alpha} - E_{\beta}$  are

$$\tilde{D}_{\alpha}(E_{\alpha} - E_{\beta}) = -\frac{\mathcal{E}_{o}^{2}}{2} \exp\{-\gamma^{2}(E_{\alpha} - E_{\beta})^{2}/8\} A_{\alpha}^{*} A_{\beta} \mathcal{Z}_{\beta\alpha},\tag{7}$$

and

$$\tilde{D}_{\beta}(E_{\alpha} - E_{\beta}) = -\frac{\mathcal{E}_o^2}{2} \exp\{-\gamma^2 (E_{\alpha} - E_{\beta})^2 / 8\} A_{\beta} A_{\alpha}^* \mathcal{Z}_{\alpha\beta}^*,\tag{8}$$

since the dipole matrix is hermitian the  $\mathcal{Z}_{\alpha\beta}^* = \mathcal{Z}_{\beta\alpha}$ , the theory predicts that the phase and amplitude of crossed terms have the same phase and amplitude. And further on normalizing all the coefficients so the zero frequency coefficient goes to unity gives a measure of the relative amplitudes between states.

This analysis also applies to continuous signal since the convolution over energy is linear on a Fourier transformation over time delay. Therefore we can compare directly with experiment

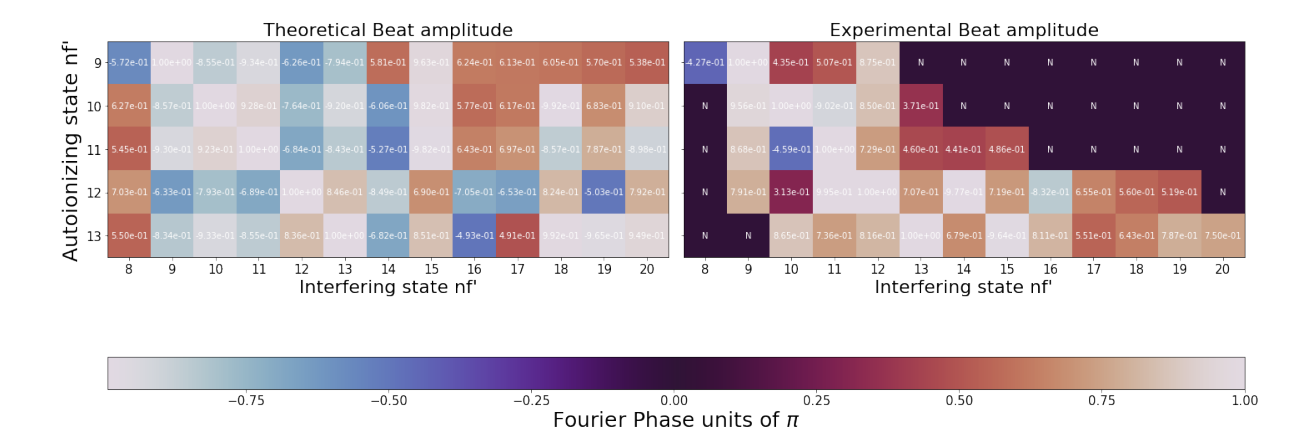


Figure 4. Phase of the quantum beats selected from FFT, in both experiment and theory. A cyclic colormap is used and the values of the phases are in units of pi. Each box has its value in a label. In this case there is a strong difference between theory and experiment. The main difference is the observed symmetry across the diagonal. In the theory plots the phases are the same across the diagonal, whereas in the experiment there is a considerable difference like in the 9-10 and 10-9 beat where the difference is almost  $\pi/2$ .

by extracting line outs from the experimental signal. This is achieved by integrating over the beating signal, but it is only reliable only for states that are separated enough to be distinguished in the spectrogram. In this case it was possible to distinguish states from n = 9 to 13.

Figure 3 shows the raw amplitudes obtained from the experimental and theoretical spectrograms. Notice that in both experiment and theory the amplitude of the coefficients is symmetric around the diagonal and the dependence on the energy separation between resonances follows a similar Gaussian structure as the theory predicts.

The phases obtained from the analysis are shown in figure 4. Here we observe that unlike the theory, the experiment does not appear to be symmetric across the diagonal. They agree on the diagonal terms being negative, but the off diagonal terms are not symmetric having difference in some cases, like the pair 9-10, of around  $\pi/2$ . The reason for this is not clear yet, but a more detailed treatment of the way these states decay into the continuum and how the phase of the electron is modified depending on the channel it decays into may solve this.

In conclusion, we obtained an electron interferogram of a wavepacket with both high temporal and spectral resolution. The essence of our metrology technique lies in the separation of temporal probing and delayed detection steps. In the case of nf' states the long autoionization lifetimes yield the required high energy resolution and while the femtosecond Raman probe pulse provides the temporal resolution. The Fourier analysis of these spectrally and temporally resolved signals enable us to determine the composition of wavepackets in terms of its constituent states. Our experimental results agree well with the second-order perturbation theory calculations. For naturally decaying states, the relaxation time determines energy resolution. However one can extend this method to bound states by employing an additional quasi-CW probe for ionization. This method will be useful for metrology of wave packets composed of a large number of densely packed states, as in the case of molecular wave packets.

Work at the University of Arizona was supported by the NSF awards PHY 2207641 and PHY 1919486, A. P. was supported by the U.S. Department of Energy, Office of Science grant DE-SC0018251. The Purdue research is supported by Award No. DE-SC0010545, also from the U.S. DOE Office of Science.

#### References

- [1] Krausz F and Ivanov M 2009 Reviews of Modern Physics 81 163-234
- [2] Remetter T, Johnsson P, Mauritsson J, Varju K, Ni Y, Lepine F, Gustafsson E, Kling M, Khan J, Lopez-Martens R, Schafer K J, Vrakking M J J and L'Huillier A 2006 Nature Physics 2 323–326
- [3] Klünder K, Johnsson P, Swoboda M, L'Huillier A, Sansone G, Nisoli M, Vrakking M J, Schafer K J and Mauritsson J 2013 Physical Review A 88 033404
- [4] Liu C and Nisoli M 2012 Physical Review A 86 033404
- [5] Han M, Ge P, Shao Y, Gong Q and Liu Y 2018 Physical Review Letters 120 073202
- [6] Li M, Xie H, Cao W, Luo S, Tan J, Feng Y, Du B, Zhang W, Li Y, Zhang Q, Lan P, Zhou Y and Lu P 2019 Physical Review Letters 122 183202
- [7] Villeneuve D M, Hockett P, Vrakking M J and Niikura H 2017 Science 356 1150-1154
- [8] Busto D, Barreau L, Isinger M, Turconi M, Alexandridi C, Harth A, Zhong S, Squibb R J, Kroon D, Plogmaker S, Miranda M, Jiménez-Galán, Argenti L, Arnold C L, Feifel R, Martín F, Gisselbrecht M, L'Huillier A and Salières P 2018 Journal of Physics B: Atomic, Molecular and Optical Physics 51 044002
- [9] Gruson V, Barreau L, Jiménez-Galan, Risoud F, Caillat J, Maquet A, Carré B, Lepetit F, Hergott J F, Ruchon T, Argenti L, Taïeb R, Martín F and Salières P 2016 Science 354 734–738
- [10] Ramswell J A, Stavros V G, Hong Q and Fielding H H 1998 Philosophical Transactions of the Royal Society A: Mathematical, Physical and Engineering Sciences 356 363–376
- [11] Månsson E P, Guénot D, Arnold C L, Kroon D, Kasper S, Dahlström J M, Lindroth E, Kheifets A S, L'Huillier A, Sorensen S L and Gisselbrecht M 2014 Nature Physics 10 207
- [12] Plunkett A, Alarcón M A, Wood J K, Greene C H and Sandhu A 2022 Phys. Rev. Lett. 128(8) 083001
- [13] Pellarin M, Vialle J L, Carré M, Lermé J and Aymar M 1988 Journal of Physics B: Atomic, Molecular and Optical Physics 21 3833–3849
- [14] Aymar M, Greene C H and Luc-Koenig E 1996 Reviews of Modern Physics 68 1015-1123
- [15] Seaton M 1983 Reports on Progress in Physics 46 167–257
- [16] Lindsay M, Dai C, Cai L, Gallagher T, Robicheaux F and Greene C 1992 Physical Review A 46 3789
- [17] Faisal F H M 1987 Theory of Multiphoton Processes (Springer US)